Original Article

# Aminated Si-Al-Fe nanocomposite on dielectrode points sensing junction: A high-performance colorectal aptasensor

Xiaogang Li[a], Ping Lu[a], Wanfu Zhang[a], Zhao Niu[a], Hongwei Wan[a], Subash C.B. Gopinath[b,c,d,e], Bo Li[a]*

[a]Department of General Surgery, The Affiliated Hospital of Yunnan University, Kunming, 650021, China
[b]Center for Global Health Research, Saveetha Medical College & Hospital, Saveetha Institute of Medical and Technical Sciences (SIMATS), Thandalam, Chennai – 602 105, Tamil Nadu, India
[c]Faculty of Chemical Engineering & Technology and Institute of Nano Electronic Engineering, Universiti Malaysia Perlis (UniMAP), 02600 Arau, Perlis, Malaysia
[d]Department of Technical Sciences, Western Caspian University, Baku AZ 1075, Azerbaijan.
[e]Department of Computer Science and Engineering, Faculty of Science and Information Technology, Daffodil International University, Daffodil Smart City, Birulia, Savar, Dhaka 1216, Bangladesh

## ARTICLE INFO

## ABSTRACT

Colorectal cancer (CRC) begins in the innermost layer of the colon or rectum. It can grow outward from this layer and spread to different parts of the body. Screening for CRC with suitable biomarkers helps to identify the early stages and improves the recovery rate. Carcinoembryonic antigen (CEA) is a widely accepted biomarker for CRC because it is overexpressed in 95% of cases, aiding in the identification and monitoring of the disease. This research developed a highly sensitive CEA biosensor on a Si-Al-Fe (Silica-Alumina-Iron) nanomaterial-modified dielectrode. In the sandwich test, CEA was captured and detected using an aptamer and an antibody. An aptamer ending with -COOH was attached to the Si-Al-Fe nanocomposite through an amine linker, which then captured the CEA and was detected with an antibody. When an aptamer was used as the capture probe rather than an antibody, the current response increased. In addition, amine-modified Si-Al-Fe increases aptamer immobilization through the reaction of amine with Si-Al-Fe and COOH in the aptamer. Si-Al-Fe modified surface provides a better arrangement of aptamer on a dielectrode. Aptamer-CEA-antibody surface identified CEA on a linear regression range of 0.3 to 20 ng/mL, and the detection limit was calculated as 0.3 ng/mL with an $R^2$ value of 0.9893. Additional complementary aptamer sequences and control proteins, such as Alpha fetoprotein (AFP) and CA15-3, did not significantly alter the responses obtained, suggesting that CEA is specifically detected. Furthermore, in serum-spiked CEA, the current response increased with rising CEA concentrations, confirming the selective identification of the antigen.

## 1. Introduction

Colorectal cancer (CRC) is a type of cancer that causes damage to the rectum or colon and has a higher mortality rate than other cancers [1]. The risk of stomach-related cancers, such as gastric and CRC, increases with age, particularly in individuals over 50 years of age [2,3]. Symptoms of CRC include blood in the stool, constipation, diarrhea, fatigue, and abdominal pain. The incidence of CRC has been decreasing in developed countries due to effective screening programs. Recovery from CRC is highly dependent on the stage of cancer, with early stages having higher survival rates than advanced stages. Timely identification, proper medication, and follow-up treatment are necessary to improve the prognosis of CRC in patients. Biomarkers play a major role in the screening and clinical management of CRC. Therefore, sensitive and rapid quantification of biomarkers is crucial for the early diagnosis of CRC.

Carcinoembryonic antigen (CEA) is a human embryonic antigen extracted first from embryonic tissue and colon cancer. CEA is expressed abnormally in CRC and is thus used widely as a biomarker for diagnosing it [4]. The normal CEA level in the serum of healthy individuals is lower than 5 μg/L; a value exceeding 20 μg/L may indicate cancer. The range

of elevation of CEA indicates whether the cancer has metastasized or is localized and helps predict outcomes. When the range falls between 5 and 10 μg/L, the rate of CRC occurrence is lower. A range greater than 1 μg/L may indicate a poor outlook with a high risk of recurrence. At the same time, the range of CEA greater than 20 μg/L indicates that the CRC can metastasize to other areas of the body. In addition, the level of CEA decreased in patients who have had surgery to remove the tumor. Physicians should, hence, do the CEA screening test on patients with CRC before and after the surgery. They should also conduct regular screening after surgery 3-month month intervals, then every six months of the first three years, and every five years to make sure the CRC does not relapse. Quantifying the level of CEA helps to identify the CRC and its condition. At present, enzyme linked immunosorbent assay (ELISA), AI based imaging, fluorescent based immunoassay and the radioimmunoassay are commonly used to quantify the CEA levels [5,6]. Still, research to develop a cheaper, easy, and highly sensitive biosensor for detecting CEA is ongoing [7-9].

A biosensor is an analytical tool that produces signals proportionate to the interactions between molecules on the detecting surface to monitor chemical and biological responses [10,11]. Biosensors are useful in many areas, including environmental monitoring, dietary

control, medication delivery, and point-of-care monitoring of illness progression [12]. Researchers are focusing on improving biosensors for sensitive detection of target molecules. Such improvement depends on various factors like the affinity of biomolecular interactions and the surface functionalization of target or analyte immobilization [13,14]. High-affinity detection molecules such as aptamers, proteins, peptides, nucleic acids, and antibodies were utilized to identify the target molecule. Among them, antibodies and nucleic acids such as DNA and RNA are commonly used as molecular detectors and successfully applied in various biosensors. Among them, aptamers are recently emerging molecules and are used for various biosensing and therapeutic applications. The aptamer is a promising molecule, a potential substitute for antibodies. It can be a DNA or RNA molecule, chemically synthesized using Systematic evolution of ligands by exponential enrichment (SELEX) method [15,16]. Due to their high-affinity target identification and 3-D folding, aptamers are considered the superior alternatives to antibodies. Apart from that, aptamers, with the advantage of easy surface modification, can be synthesized without animal routes and are cost-effective and stable. Due to this positive feature, aptamers are utilized as detection molecules for various sensors and help to diagnose diseases. Here, a CEA specific aptamer was used to create a CEA biosensor on nanomaterial modified dielectrode points sensing surface, to monitor CRC.

Nanotechnology has become the most developed field in the areas of engineering, chemistry, biology, physics, medicine and forensics [17-21]. Nanomaterial application in the biomedical field offers potential opportunities in the treatment of damaged tissue, bone cancer, neurodegenerative disorders, infection, cancer, and other diseases [22,23]. Organic nanomaterials such as liposomes, organic polymers, dendrimers, and hydrogel nanomaterials have been generated for various biomedical applications. Nanomaterials' application in surface functionalization of biosensors is playing a crucial role in improving sensing strategies. Enhancing the stability of biomolecules on the electrode and optimizing their arrangement can lead to improved analytical results and a reduction in the detection limit [24,25]. Various types of biosensors are developed with nanomaterials to target cancer biomarkers. For instance, cancer antigens 15-3 are effectively focused with a nanomaterial-based electrochemical sensor for diagnosing breast cancer [26]. Gold nanobiosensors are becoming popular for treating and diagnosing breast cancer. These sensors identify protein markers of cancer by utilizing the nanoscale characteristics of gold particles, and this method enables the early and more precise identification of breast cancers [27]. Apart from that, a novel composite of graphene oxide (2D) and graphitic carbon nitride decorated with gold nanoparticles is used for the sensitive detection of prostate-specific antigen (PSA) by using an aptamer-based electrochemical biosensor. The biosensor achieved rapid detection of PSA at 30 mins, and its potential for clinical use was further validated by analyzing real serum samples [28]. Similar to other cancer detections, nanomaterials have transformed the detection and treatment of CRC, making disease management more accurate and effective. Nanomaterials are conjugated with the desired ligand that targets the CRC biomarkers and enables detection. Biomarkers such as CA19-9, TP53, and CEA are detected with higher sensitivity by nanomaterial-based biosensing systems [29]. Here, Si-Al-Fe nanomaterial extracted from the fly ash was used to attach the anti-CEA aptamer to the dielectrode. Silica is commonly used in biosensors due to its larger surface area and optical properties. Due to its highly selective nature of the recognition of the target molecules, silica has been reported for various biosensors to identify biomolecules such as DNA, antibodies, and viruses [30]. Aluminum is one of the established materials known for its high sensitivity, specificity, and reusability, which enhance the properties of sensing devices [31]. Iron oxide, due to its low toxicity and unique biocompatibility, is widely used for drug delivery in cancer therapies. Additionally, iron has been extensively utilized in biosensor applications, such as Bisphenol A (BPA) sensors, glucose sensors, and gas sensors [32]. In this research, a combination of Si-Al-Fe was prepared for the surface functionalization of a CEA biosensor for diagnosing CRC.

## 2. Materials and Methods

### 2.1. Reagents and biomolecules

Anti-CEA antibodies, CEA, carbohydrate antigen 15-3 (CA15-3), and alpha-fetoprotein (AFP) were purchased from Beijing Dingguo Changsheng Biotechnology Co. Ltd, China. Phosphate buffered solution (PBS), Human serum, (3-Aminopropyl) triethoxysilane (APTES), and PEG-COOH were ordered from Sigma Aldrich, USA. Anti-CEA aptamer was commercially synthesized and received from a local supplier. The dielectrode points junction sensing surface was fabricated as described earlier by the photolithographic technique and verified by a scanning electron microscope image [33].

### 2.2. Si-Al-Fe extraction from fly ash

Si-Al-Fe nanomaterial was synthesized using the extracted silica, alumina and iron from the coal mine fly ash. Three major steps are involved in this process. (i) Extraction of Fe; (II) extraction of sodium aluminosilicate; (iii) Si-Al-Fe synthesized by Sol-gel method.

### 2.3. Fe extraction from fly ash

Using a magnetic stirrer, fly ash (25 g) was mixed with distilled water (500 μL) and swirled for 15 mins. The stacked Fe was collected on the magnetic rod. The process was repeated until all Fe particles were extracted from the fly ash. Next, 20 % $H_2SO_4$ was combined with the separated Fe particles (1 g), and the mixture was agitated for two hrs at 60 °C. After passing through a Whatmann filter paper, the Fe-containing solution was utilized as the foundation for synthesis of Si-Al-Fe nanomaterials.

### 2.4. Sodium aluminosilicate extraction

Alkaline extraction was followed by using sodium aluminosilicate from fly ash. First, 100 g of the fly ash was combined with 2 L of NaOH (2.5 M), and this combination was heated for 5 hrs at 100 °C while being stirred. A Whatmann filter paper was used to separate the sodium alumina-silicate solution once it had cooled. Si-Al-Fe nanomaterials were synthesized by using this solution as a foundation.

### 2.5. Si-Al-Fe synthesizes by sol gel method

Si-Al-Fe nanomaterial was synthesized by using the sol-gel method. At first, 500 mL of sodium aluminosilicate (extracted from fly ash) was placed into a beaker and stirred. Extracted Fe solution was further added drop-by-drop until pH 7 was reached and the gel was formed. The gel was stirred overnight to get a uniform distribution of nanomaterials. Further, the gel was rinsed with ethanol and distilled water and separated by centrifugation (10000 rpm for 10 min). The final Si-Al-Fe nanomaterial was dried at 100 °C and kept at room temperature (RT).

### 2.6. Amine modification on Si-Al-Fe nanomaterial

Si-Al-Fe nanomaterial was modified into amine by silane coupling. Briefly, 1 mg/mL of Si-Al-Fe was dispersed in 1 % KOH (10 min) and then washed with distilled water. The nanomaterials were separated by centrifugation. After that 2 % of APTES was introduced in the nanomaterial and heated at 300 °C. After that, the nanomaterials were rinsed with ethanol and separated by centrifugation.

### 2.7. Optimization of antibody in antibody-CEA-aptamer sandwich assay

Antibody-CEA-aptamer assay was conducted on Si-Al-Fe modified IDME. For this process, IDME was immersed in KOH and distilled water was used to remove the excess KOH. After that, amine-modified Si-Al-Fe was added on the surface and the electrode was kept at room temperature (RT) for 3 hrs to enable APTES attachment to KOH. Further, an antibody concentration of 50 nM was introduced to the electrode for 1 hr to interact the antibody with the amine-modified Si-Al-Fe. PEG-COOH was added to block the uncovered amine surfaces, followed by CEA (20 ng/mL). It was then allowed to rest (30 min) to

allow the binding of CEA with its antibody. Finally, a fixed aptamer (1 µM-diluted in PBS) was added to make the sandwich assay of antibody-CEA-aptamer. In between each process, the electrode was rinsed with PBS to clear the unbound chemicals and biomolecules. The same experiment was conducted with other antibody concentrations such as 100, 200, 400, 800, and 1600 nM.

## 2.8. Optimization of aptamer in aptamer-CEA-antibody sandwich

Aptamer-CEA-antibody was performed on Si-Al-Fe modified sensing surface. After treatment with KOH, amine modified Si-Al-Fe was added on the surface of the electrode kept at RT for 3 hrs to allow attachment of APTES on KOH. Further, a COOH-aptamer (50 nM) was introduced to the electrode and rested for 1 hr to interact the antibody with the amine-modified Si-Al-Fe. PEG-COOH was added to block the uncovered amine surfaces and then CEA (20 ng/mL) was added. Finally, a fixed antibody concentration of 400 nM was added to make the sandwich assay of aptamer-CEA-antibody. The surface was washed with PBS in between each immobilization and the current changes were recorded. The same experiment was conducted with other aptamer concentrations such as 100, 200, 400, 800, and 1600 nM (diluted in PBS).

## 2.9. Detection limit of CEA

The CEA limit of detection was calculated by titrating CEA from 0.6 to 20 ng/mL. The following steps are involved in this process. (i) bare surface was immersed in KOH for 15 min; (ii) Si-Al-Fe was added on the surface and rested for 3 hrs; (iii) optimized COOH-aptamer was added; (iv) PEG-COOH wad placed on the electrode (iv) 5 µL of CEA from 0.312 to 20 ng/mL was introduced; (v) optimized anti-CEA was added. The current level was recorded before and after adding CEA. The difference in current was plotted in a linear regression line to calculate the detection limit of CEA.

## 2.10. Control experiments with CA15-3, AFP and complementary aptamer

Control experiments were conducted with AFP, CA15-3, and complementary anti-CEA aptamer. Instead of CEA, AFP and CA15-3 were added to the aptamer-modified IDME, followed by the addition of the anti-CEA antibody. In another experiment, the -COOH ended complementary was added on the Si-Al-Fe modified IDME and then CEA (20 ng/mL) followed by anti-CEA was added. The current responses were monitored in all these three experiments and compared with specific sandwich assay with CEA, anti-CEA aptamer, and anti-CEA antibody.

## 2.11. Detection of serum spiked CEA and the stability of sensing electrode

An aptamer-CEA-antibody sandwich assay was used to quantify serum-spiked CEA to determine its detection condition from biological samples. CEA was diluted in 10% human serum to a concentration of 0.32 to 20 ng/mL, put onto a sensing surface that had an aptamer linked to it, and then sandwiched with an anti-CEA antibody. Every serum spiking CEA concentration had a documented current reaction. To identify the stability of the sensing electrode, dielectrode points sensor modified with Si-Al-Fe and aptamer was tested at the intervals of 1, 4, 8, 16, and 32 weeks. For this experiment, the same batch of dielectrode points sensing surface was surface functionalized with the aptamer and kept in the refrigerator. On these aptamers modified surfaces CEA was added and then sandwiched with anti-CEA antibody. Any changes of current were noted and compared. Further, stability analysis was performed on aptamer modified Si-Al-Fe electrodes with different time intervals. For this process, the aptamer modified electrodes were kept in the refrigerator for 1-, 2-, 3- and 4-weeks. The sandwich assay was performed with the electrodes for CEA detection and the current responses were recorded. All experiments were performed at room temperature under ambient humidity. The surface of sensors was kept wet [by 10 mM PBS (pH 7.4)] during the biomolecular interactive analysis. Washings were carried out between each step or modification using 10 reaction volume of PBS. To cover the gap region 5 µL of sample was used for each reaction. Power supply was provided by a
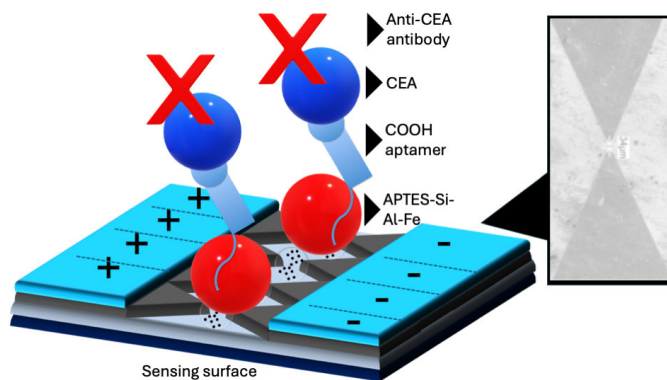


**Figure 1.** Schematic illustration of Carcinoembryonic antigen (CEA) biosensor on dielectrode points sensor. The dielectrode points sensor was initially immersed in KOH, and then the surface of the electrode was modified with Si-Al-Fe using an (3-Aminopropyl) triethoxysilane (APTES) as a amine linker. After that, aptamer ended with -COOH was added, followed by the addition of CEA. Finally, an anti-CEA antibody was interacted to make a sandwich with aptamer-CEA-antibody. Dielectrode points junction is displayed with a scanning electron microscope image.

picoammeter at the range of 0-2 V with the sweep of 0.1 V on the dual electrode probe station.

## 3. Results and Discussion

CRC starts in the rectum or colon. Diagnosing this cancer with suitable biomarkers is essential to provide better treatment and improve the quality of life. Here, we introduced a highly sensitive CEA biosensor for diagnosing CRC. Figure 1 shows a schematic illustration of the CEA biosensor on dielectrode points sensor and the surface imaging under scanning electron microscope. The sensing surface is initially immersed in KOH, and then the surface of the electrode was modified with Si-Al-Fe using an APTES amine linker. After that, an aptamer (or antibody) ending with -COOH was added, followed by the addition of CEA. Finally, an anti-CEA antibody (or anti-CEA aptamer) was added to create the sandwich assay of aptamer-CEA-antibody or antibody-CEA-aptamer. For surface functionalization, Si-Al-Fe was used to attach the aptamer or antibody to the sensing electrode. Various research studies have shown that nanomaterials enhance biomolecule attachment and improve the stability of the molecules on the sensing surfaces [34]. The dielectrode fabricated in this study was made up of two independently bright electrodes arranged in a triangular pattern, which showed a better potential for developing a highly sensitive biosensor than the conventional parallel electrodes. In addition, surface functionalization on dielectrode plays a major role in improving the sensitivity of the sensor. To improve the aptamer immobilization, Si-Al-Fe was utilized as a nanocomposite. Si-Al-Fe modified dielectrode provides a better arrangement of aptamers with higher stability on the sensing surface, which interacts with a higher number of CEAs, and increases the sensitivity. Apart from this, Si-Al-Fe modified electrodes increase the current flow upon interaction of CEA with its aptamer and antibody, which lowers the detection limit. When the antibody is directly attached to the APTES surface, there is a limited number of antibodies that can bind to the surface. At the same time, on the single Si-Al-Fe nanomaterial many APTES molecules are attached and attract more antibodies, which improves the capture biomolecule immobilization and helps lower the detection limit. This modified sensor identifies the lower level of CEA.

## 3.1. Surface morphology of Si-Al-Fe

Imaging of synthesized Si-Al-Fe was analyzed by field emission scanning electron microscopy (FESEM) and field emission transmission electron microscopy (FETEM). Figure 2(a) and 2(b) shows the FESEM image of Si-Al-Fe with the magnitude of 1 µm and 200 nm, respectively. Nanomaterials are uniformly distributed and sized within the range of 20-30 nm. The FETEM image also clearly shows the distributed nanomaterial with uniform arrangement (Figure 2c). The electron
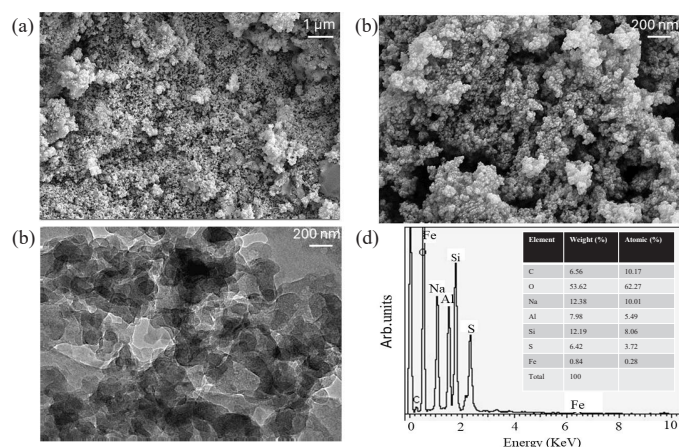
**Figure 2.** Characterization of Si-Al-Fe. (a) Field emission scanning electron microscopy (FESEM) image of Si-Al-Fe with the scale at 1 μm. (b) Field emission transmission electron microscopy (FETEM) with 200 nm scale. (c) FETEM with 200 nm scale. Nanomaterials are uniformly distributed and sized within the range of 20-30 nm. (d) Energy-dispersive X-ray (EDX) of Si-Al-Fe. EDX result confirms the presence of the major elements of Si, Al, Fe, and O in the synthesized material.
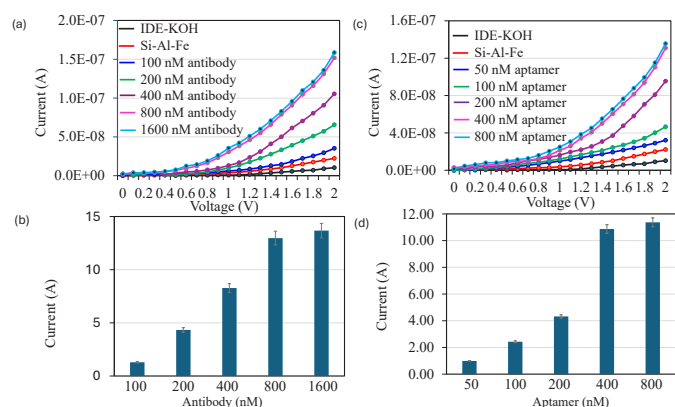


**Figure 3.** Comparison of aptamer and antibody attachment on dielectrode points sensor. (a) Current-volt graph of different concentration of antibody attachment on dielectrode points sensor and shows a clear increment of current after introducing each antibody. (b) Current response of antibody attachment on dielectrode points sensor. With increasing the concentration of antibodies, current response also increased and saturated at 800 nM (c) Current-volt graph of different concentrations of antibody attachment on dielectrode points sensor and shows a clear increment of current after introducing aptamer. (d) Current response of aptamer attachment on dielectrode points sensor. With increasing concentrations of antibodies, current responses also increased and saturated at 400 nM. Data was averaged by averaging three independent measurements using the sensing surfaces prepared from the same batch of fabrication.

dispersive X-ray (EDX) result confirms the presence of the major elements Si, Al, Fe, and O in the synthesized material (Figure 2d).

### 3.2. Comparison of aptamer and antibody attachment on Si-Al-Fe modified dielectrode points sensor

Capture probe immobilization plays a major role in improving the biosensor. The interaction of capture and target is also important for lowering the detection limit. Here, an antibody and aptamer were used to detect CEA. To identify the suitable capture probe, two different types of experiments were conducted: antibody-CEA-aptamer and aptamer-CEA-antibody.

### 3.3. Antibody immobilization on dielectrode points sensor

In the sandwich assay of antibody-CEA-aptamer, to immobilize the higher number of antibodies, different concentrations of antibody immobilization were tested on the Si-Al-Fe modified dielectrode points sensor. Figure 3(a) shows the current-volt graph of different concentrations of antibody attachment on the dielectrode points sensor. As shown in the figure, the dielectrode points sensor-KOH shows the current response as 1.03 E-08 A, which after the addition of amine-modified Si-Al-Fe current, changed to 2.23 E-08 A. This indicates the modification of the electrode with the nanomaterial Si-AL-Fe. After that antibody with 100 nM was added, the current was increased to 3.52 E-08 A, which indicates attachment of the anti-CEA antibody to the amine-modified Si-Al-Fe. On increasing the concentration of antibodies to 200, 400, 800, and 1600 nM, the current level increased to 6.56 E-08 A, 1.05 E-07 A, 1.52 E-07 A, and 1.59 E-07 A, respectively. It clearly showed that the increment in current responses is by increasing the antibody concentration. The differences in current before and after antibody attachment with 100, 200, 400, 800, and 1600 nM were 1.29, 4.33, 8.27, 12.97, and 13.67 E-08 A, respectively (Figure 3b). The current response was saturated from 800 nM; this indicated that a maximum of 800 nM of the antibody is enough to cover the Si-Al-Fe modified dielectrode points sensor surface. On these surfaces, an antibody-CEA-aptamer sandwich assay was conducted.

### 3.4. Aptamer immobilization on dielectrode points sensor

In the sandwich assay of aptamer-CEA-antibody, to immobilize the higher number of aptamers, different concentrations of aptamer immobilization were tested on the Si-Al-Fe modified dielectrode points sensor. Figure 3(c) shows the current-volt graph of different concentrations of aptamer attachment on the dielectrode points sensor. As shown in figure, dielectrode points sensor-KOH shows the current response as 1.04 E-08 A. After the addition of amine, modified Si-Al-Fe

current was changed to 2.25 E-08 A, which implies the modification of the electrode with the nanomaterial Si-AL-Fe. After that aptamer with 50 nM was added and the current was increased to 3.22 E-08 A, which indicates the attachment of anti-CEA aptamer on the amine-modified Si-Al-Fe. Increased the concentration of aptamers to 100, 200, 400, and 800 nM, the levels of current were increased to 4.66 E-08 A, 9.55 E-08 A, 1.31 E-07 A, and 1.36 E-07 A, respectively. This clearly showed that the increment of current responses was due to increasing the aptamer concentration. The differences in current before and after aptamer attachment with 50, 100, 200, 400, and 800 nM were 0.99, 2.43. 4.32, 10.09, and 11.4 E-08 A, respectively (Figure 3d). The current response was saturated to 400 nM, indicating that the maximum aptamer concentration was enough to cover the Si-Al-Fe modified dielectrode points sensor surface. On these surfaces, an aptamer-CEA-antibody sandwich assay was conducted.

### 3.5. Comparison detection of CEA on aptamer-CEA-antibody and antibody-CEA-aptamer sandwich assay

On the aptamer- and antibody-optimized surfaces, CEA was detected by aptamer-CEA-antibody and antibody-CEA-aptamer sandwich assay (Figure 4). Figures 4(a) and 4(b) show the current-volt graph of 20 ng/mL of CEA detection by antibody-CEA-aptamer and aptamer-CEA-antibody sandwich assay. As shown in Figure 4(c) the difference of current response was higher in the aptamer-CEA-antibody assay. This may be due to the higher binding affinity of aptamer with CEA compared with antibody. Aptamers exhibit superior sensitivity and selectivity towards target molecules in comparison to antibodies, as demonstrated by numerous studies. When paired with antibodies, the aptamer can draw in more targets and enhance the existing reactions when employed as the capture molecule.

### 3.6. Detection limit of CEA

Since aptamer as the capture probe increases the current flow for the CEA detection, different concentrations of CEA were tested with aptamer-CEA-antibody sandwich assay. CEA was diluted and dropped on an aptamer immobilized electrode and then sandwiched with anti-CEA antibody. Figure 5(a) shows the current-volt measurement of CEA from 0.6 to 20 ng/mL detection by aptamer-CEA-antibody assay. With zero CEA, the current response was recorded as 1.26 E-07 A. After introducing CEA with 0.6 ng/mL, the current was increased to 3.01 E-07 A. This increment of current confirms the binding of CEA with its aptamer and antibody. Furthermore, with an increase in the concentration of CEA to 1.2, 2.5, 5, 10, and 20 ng/mL, the current
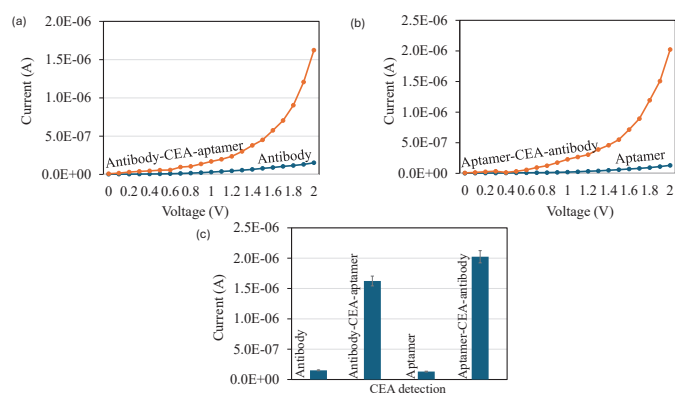
**Figure 4.** Detection of Carcinoembryonic antigen (CEA) by aptamer and antibody. (a) Current-volt measurement graph of CEA detection by antibody-CEA-aptamer sandwich. The current increment was confirmed the CEA interaction with antibody and aptamer. (b) Current-volt measurement graph of CEA detection by aptamer-CEA-antibody sandwich assay. Current increment was confirmed the CEA interaction with aptamer and antibody. (c) Comparative detection of CEA by aptamer and antibody as the capture probe. Clearly seen that the current response was increased when aptamer was used as the capture probe. Data was averaged by averaging three independent measurements using the sensing surfaces prepared from the same batch of fabrication.
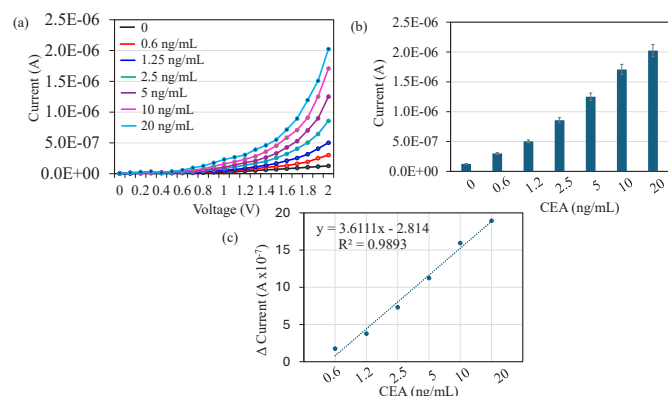


**Figure 5.** Detection limit of Carcinoembryonic antigen (CEA). (a) Current-volt graph with different concentrations of CEA interaction with aptamer and antibody. A clear increment of current was noticed after introducing each CEA concentration. (b) Current response of CEA interaction with aptamer and antibody. Clear increments of current response were recorded for all the concentrations of CEA, and it proportionally increased by increasing concentrations of CEA. (c) Difference in current before and after CEA detection was plotted in an Excel spreadsheet and calculated for the detection of CEA as 0.6 ng/mL with the R-squared value of 0.9893. Data was averaged by averaging three independent measurements using the sensing surfaces prepared from the same batch of fabrication.

response increased to 5.03 E-07 A, 8.57 E-07 A, 1.25 E-06 A, 1.71 E-06 A, and 2.02 E-06 A. Clear increments of current response were recorded for all concentrations of CEA and it proportionally increased by increasing the concentration of CEA (Figure 5b). The difference in current before and after CEA detection was plotted in an excel spreadsheet and calculated. The detection of CEA was 0.6 ng/mL with the R-squared value of 0.9893 (Figure 5c). This lower-level detection limit was achieved through the higher-level immobilization of aptamer on the dielectrode points sensor through the Si-Al-Fe nanomaterial.

### 3.7. CEA detection from CEA-spiked human serum

By using an aptamer-CEA-antibody sandwich assay, CEA was spiked in human serum to determine the effectiveness of CEA detection in the real-world sample. The current response of CEA detection, which increased as CEA concentrations rose, is shown in Figure 6(a) and ranges from 0.6 ng/mL to 20 ng/mL. This confirms the CEA detection in the human serum without any interference. The presence of other proteins in human serum, such as albumin and globulin, may potentially obstruct CEA's ability to interact with its aptamer and antibody. Since aptamer was employed as the capture probe, the current response is increased and the CEA in the human serum is preferentially recognized.
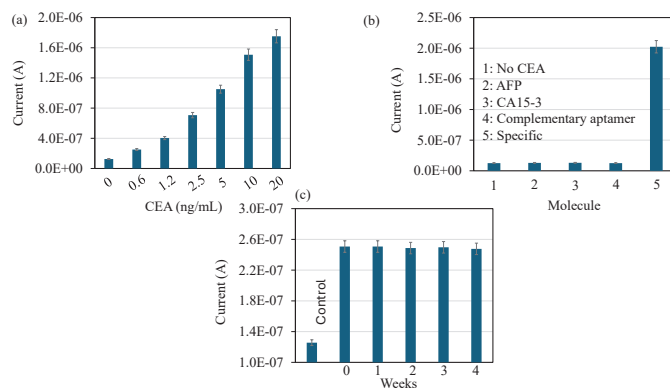


**Figure 6.** (a) Carcinoembryonic antigen (CEA) detection in CEA-spiked human serum. Different concentrations of CEA were spiked in human serum and detected by aptamer-CEA-antibody sandwich. Aptamers selectively recognized the CEA in human serum and increased the current response. (b) Specific identification of CEA. Experiments were performed with control proteins Alpha fetoprotein (AFP), cancer antigen 15-3 (CA15-3), and complementary anti-CEA aptamer. The current responses for the control experiments did not show any significant changes, which confirms the specific identification of CEA. (c) Stability analysis for CEA detection. CEA was detected on aptamer-modified surfaces at intervals of 1 to 4 weeks. There were no differences in current responses for all the electrodes, indicating that the aptamer-modified electrodes are more stable and detected CEA without losing sensitivity. Data was averaged by averaging three independent measurements using the sensing surfaces prepared from the same batch of fabrication.

The normal level of CEA in a healthy human is less than 5 mcg/L, if it is more than 20 mcg/L in the human serum may be the indicator of cancer. Here the clear increment of current response was indicated from 0.3 ng/mL to 20 ng/mL, which helps to identify colorectal cancer.

### 3.8. Specific detection of CEA

Specific identification of CEA was analyzed on the Si-Al-Fe modified dielectrode points sensor using the control proteins and complementary aptamer. Experiments were performed with control proteins AFP, CA15-3, and complementary anti-CEA aptamer. Instead of CEA, AFP and CA15-3 were added to the anti-CEA aptamer attached IDME, followed by adding an anti-CEA antibody. In another experiment, -COOH ended complementary was used instead of anti-CEA aptamer. The current responses were monitored in all three experiments. The current responses for control experiments did not show any significant changes, which confirms the specific identification of CEA (Figure 6b). In the stability analysis, CEA was detected on the aptamer-modified surfaces at intervals of 1 to 4 weeks. As shown in Figure 6(c), no difference in current responses was recorded for all the electrodes, indicating that aptamer-modified electrodes were more stable and detected CEA interaction without losing sensitivity (Figure 6c).

## 4. Conclusions

CRC is a type of cancer that starts in the colon or rectum. Biomarkers play a vital role in CRC diagnosis, treatment, and prognosis. In this research, a CEA biosensor was developed on a Si-Al-Fe modified dielectrode points sensor. The Si-Al-Fe modified surface helps enhance the capture probe of aptamer immobilization. Aptamers and antibodies were compared as capture probes detect CEA, and it was found that the current response was increased when an aptamer was used as the capture probe compared to an antibody. The aptamer-CEA-antibody sandwich assay increased current response more than the antibody-CEA-aptamer assay for the same concentration of CEA. The current response gradually increased with increasing CEA concentrations from 0.6 ng/mL to 20 ng/mL, with a detection limit of 0.6 ng/mL and an r-squared value of 0.9893. Further, CEA-spiked serum was detected by the aptamer-CEA-antibody sandwich assay without any interferences. Control experiments with proteins AFP, CA15-3, and complementary anti-CEA aptamer did not show any significant changes in current responses, indicating the specific detection of CEA. This aptamer-CEA-antibody sandwich assay on the Si-Al-Fe modified dielectrode points sensor identifies CEA at low levels and helps diagnose and monitor the

condition of CRC. The demonstrated dielectrodes provide a potential and common platform for analyzing other clinical biomarkers. Further, optimizing the sensing surface with other nanomaterials or nanocomposites will reveal a great sensing surface for high-performance analysis. The current sensor uses a gap region at the micromolar scale. Further reduction to a nanoscale level without a short-circuit would be a fined-tuned sensing surface.

## CRediT authorship contribution statement

**Xiaogang Li and Ping Lu:** Data curation, Formal analysis, Investigation, Writing original draft preparation; **Wanfu Zhang and Zhao Niu:** Data curation, Methodology, Writing-Reviewing and Editing; **Hongwei Wan:** Data curation, Validation, Writing-Reviewing and Editing; **Subash C.B. Gopinath:** Validation, Visualization, Writing-Reviewing and Editing; **Bo Li:** Conceptualization, Project administration, Funding acquisition, Resources, Writing-Reviewing and Editing.

## Declaration of competing interest

The authors declare no competing interest.

## Declaration of Generative AI and AI-assisted technologies in the writing process

The authors confirm that there was no use of artificial intelligence (AI)-assisted technology for assisting in the writing or editing of the manuscript and no images were manipulated using AI.

## Funding

## References

1. Zhang, X., Hu, F., Li, G., Li, G., Yang, X., Liu, L., Zhang, R., Zhang, B., Feng, Y., 2018. Human colorectal cancer-derived mesenchymal stem cells promote colorectal cancer progression through IL-6/JAK2/STAT3 signaling. *Cell Death Diseases* **9**, 25. https://doi.org/10.1038/s41419-017-0176-3

2. Wang, J., Zhao, Y., Li, P., Zhang, S., 2022. Advances in the application of regenerative medicine in prevention of post-endoscopic submucosal dissection for esophageal stenosis. *Journal of Translational International Medicine* **10**, 28-35. https://doi.org/10.2478/jtim-2022-0011

3. Sun, K., Lv, H., Chen, B., Nie, C., Zhao, J., Wang, S., Wang, J., Xu, W., Chen, X., 2021. Dawning precision treatment for gastric cancer: The latest biomarkers. *Journal of Translational International Medicine* **9**, 228-230. https://doi.org/10.2478/jtim-2021-0023

4. David, B., James F, R., 2019. Specific conductance chapter 6.3 of section A, national field manual for the collection of water-quality data.

5. Gopinath, N., 2023. Artificial intelligence and neuroscience: An update on fascinating relationships. *Process Biochemical* **125**, 113-120. https://doi.org/10.1016/j.procbio.2022.12.011

6. Gopinath, N., 2021. Artificial intelligence: Potential tool to subside SARS-CoV-2 pandemic. *Process Biochemical* **110**, 94-99. https://doi.org/10.1016/j.procbio.2021.08.001

7. Wang, J., Hua, X., Jin, B., 2022. Ultrasensitive detection of carcinoembryonic antigen by chitosan/Polythiophene/CdTe electrochemical biosensor. *ACS Omega* **7**, 45361-45370. https://doi.org/10.1021/acsomega.2c05950

8. Mohammadniaei, M., Zhang, M., Qin, X., Wang, W., Pia, L., Gürbüz, H., Helalat, S., Naseri, M., Sun, Y., 2024. A hand-held electrochemiluminescence biosensor for detection of carcinoembryonic antigen. *Talanta* **266**, 125087. https://doi.org/10.1016/j.talanta.2023.125087

9. Ibrahim, M., Greish, Y., 2023. MOF-Based biosensors for the detection of carcinoembryonic antigen: A concise review. *Molecules* **28**, 5970. https://doi.org/10.3390/molecules28165970

10. Gopinath, S. C. B., Xuan, S. 2021. DNA–RNA Complementation on silicon wafer for thyroid cancer determination. *Biotechnology Applied Biochemistry* **68**, 554–559. https://doi.org/10.1002/bab.1961.

11. Song, F., Yang, Y., Gopinath, S., 2021. Silica nanoparticle assists determining liver cancer gene sequence on interdigitated electrode surface. *Biotechnology Applied Biochemistry* **68**, 683-689. https://doi.org/10.1002/bab.1980

12. Iversen, M., Monisha, M., Agarwala, S., 2021. Flexible, wearable and fully-printed smart patch for pH and hydration sensing in wounds. *International Journal of Bioprinting* **8**, 447. https://doi.org/10.18063/ijb.v8i1.447

13. Lakshmipriya, T., Horiguchi, Y., Nagasaki, Y., 2014. Co-immobilized poly(ethylene glycol)-block-polyamines promote sensitivity and restrict biofouling on gold sensor surface for detecting factor IX in human plasma. *Analyst* **139**, 3977-85. https://doi.org/10.1039/c4an00168k

14. Lakshmipriya, T., Fujimaki, M., Gopinath, S., Awazu, K., Horiguchi, Y., Nagasaki, Y., 2013. A high-performance waveguide-mode biosensor for detection of factor IX using PEG-based blocking agents to suppress non-specific binding and improve sensitivity. *Analyst* **138**, 2863-70. https://doi.org/10.1039/c3an00298e

15. Lakshmipriya, T., Gopinath, S.C.B., 2018. Aptamer: A versatile probe in medical diagnosis. *INNOSC Theranostics and Pharmacological Sciences* **1**, 14–19. https://doi.org/10.26689/itps.v1i1.511.

16. Gopinath, S., 2007. Antiviral aptamers. *Archives of Virology* **152**, 2137-57. https://doi.org/10.1007/s00705-007-1014-1

17. Sonia Fathi, K., Easwaran Chonnur, E., Zelal, K., Abbas, R., Sadanand, P., 2024. Unlocking mysteries: The cutting edge fusion of nanotechnology and forensic science. *Bionanoscience* **14**, 3572–3598.

18. Pourmadadi, M., Eshaghi, M.M., Ostovar, S., Shamsabadipour, A., Safakhah, S., Mousavi, M.S., Rahdar, A., Pandey, S. 2022. UiO-66 metal-organic framework nanoparticles as gifted MOFs to the biomedical application: A comprehensive review. *Journal of Drug Delivery Science and Technology* **76**, 103758. https://doi.org/10.1016/j.jddst.2022.103758.

19. Kushwaha, A., Goswami, L., Kim, B., 2022. Nanomaterial-Based therapy for wound healing. *Nanomaterials (Basel)* **12**, 618. https://doi.org/10.3390/nano12040618

20. Yun, Y., Eteshola, E., Bhattacharya, A., Dong, Z., Shim, J., Conforti, L., Kim, D., Schulz, M., Ahn, C., Watts, N., 2009. Tiny medicine: Nanomaterial-based biosensors. *Sensors (Basel)* **9**, 9275-99. https://doi.org/10.3390/s91109275

21. Jiang, C., Lan, L., Yao, Y., Zhao, F., Ping, J., 2018. Recent progress in application of nanomaterial-enabled biosensors for ochratoxin a detection. *TrAC, Trends in Analytical Chemistry* 236–249. https://doi.org/10.1016/j.trac.2018.02.007.

22. Sarvari, P., Sarvari, P., 2023. Advances in nanoparticle-based drug delivery in cancer treatment. *Global Translational Medicine* **2**, 0394. https://doi.org/10.36922/gtm.0394.

23. Yusoff, M.S., Gopinath, S.C.B., Uda, M.N.A., Lakshmipriya, T., Wan Yaakub, A.R., Anbu, P., 2022. Conjugation of silver and gold nanoparticles for enhancing antimicrobial activity. *INNOSC Theranostics and Pharmacological Sciences* **4**, 38–47. https://doi.org/10.36922/itps.v4i2.70.

24. Qin, D., Gong, Q., Li, X., Gao, Y., Gopinath, S., Chen, Y., Yang, Z., 2023. Identification of mycoplasma pneumoniae by DNA-modified gold nanomaterials in a colorimetric assay. *Biotechnology Applied Biochemistry* **70**, 553-559. https://doi.org/10.1002/bab.2377

25. Gu, D., Zhang, Q., Guo, J., Ma, T., Li, H., Ji, J., Gopinath, S.C.B., Lakshmipriya, T., Li, S., Shen, D. 2020. Gold nanomaterial hybrid on PEGylated metal oxide interdigitated mini-electrode surface to diagnose prostate cancer. *Nano* **15**, 2050154. https://doi.org/10.1142/S1793292020501544.

26. Mehrab, P., Amirhossein, G., Amirhossein, K., Fatemeh, Y., Yasin, M., Rabia, A., Abbas, R., 2024. Breast cancer detection based on cancer antigen 15-3, emphasis on optical and electrochemical methods: A review. *Biosensors and Bioelectronics* **260**, 116245.

27. Soheil, S., Ashkan, H., Abbas, R., Sadanand, P., Parian, P. J., Narges, L., Mahdi, S., Shahla, S. K., Zelal, K., Sonia, F.-K., Hassan, B., 2024. Gold nanobiosensors and machine learning: pioneering breakthroughs in precision breast cancer detection. *European Journal of Medicinal Chemistry Reports* **12**, 100238.

28. Fatemeh Saeidi, T., Mehrab, P., Fatemeh, Y., Hamid, R., Abbas, R., Sonia, F., Luiz Fernando, R. F. 2024. Ultrasensitive aptamer-based electrochemical nanobiosensor in diagnosis of prostate cancer using 2D: 2D reduced graphene oxide/graphitic carbon nitride decorated with Au nanoparticles. *European Journal of Medicinal Chemistry Reports* **12**, 100192.

29. Ashkan, H., Soheil, S., Abbas, R., Mansour, B., Narges, L., Shiva, D., Arezou, R., Soroush Partovi, M., Khashayar, H., 2024. Exploring the integration of nanotechnology in the development and application of biosensors for enhanced detection and monito of colorectal cancer. *Inorganic Chemistry Communications* **164**, 112409.

30. Prabha, S., Durgalakshmi, D., Rajendran, S., Lichtfouse, E., 2021. Plant-derived silica nanoparticles and composites for biosensors, bioimaging, drug delivery and supercapacitors: A review. *Environmental Chemistry Letters* **19**, 1667-1691. https://doi.org/10.1007/s10311-020-01123-5

31. Afnan Uda, M.N., Jambek, A.B., Hashim, U., Uda, M.N.A., 2020. Electrical DNA biosensor using aluminium interdigitated electrode for salmonella detection. *IOP Conference Series: Materials Science and Engineering* **743**, 012022. https://doi.org/10.1088/1757-899X/743/1/012022.

32. Singh, A., Kumar, V., 2020. Iron oxide nanoparticles in biosensors, imaging and drug delivery applications—A complete tool. In: Balas, V., Solanki, V., Kumar, R., editor. Intelligent of Things and Big Data Applications, Vol. **180**, p. 243–252. https://doi.org/10.1007/978-3-030-39119-5_20.

33. Balakrishnan, S., Hashim, U., Gopinath, S., Poopalan, P., Ramayya, H., Veeradasan, P., Haarindraprasad, R., Ruslinda, A., 2016. Polysilicon nanogap lab-on-chip facilitates multiplex analyses with single analyte. *Biosens. Bioelectron.* **84**, 44-52. https://doi.org/10.1016/j.bios.2015.10.075

34. Hayat, A., Catanante, G., Marty, J., 2014. Current trends in nanomaterial-Based amperometric biosensors. Sensors (Basel) 14, 23439-23461. https://doi.org/10.3390/s141223439